Light-harvesting properties of photocatalyst supports—no photon left behind

Check for updates
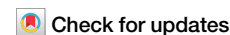
Athanasios A. Tountas[1], Anselm Dreher[2,7], Wenjie Zhou[3,7], Abhinav Mohan[4], Nazir P. Kherani[5], Geoffrey A. Ozin[6] ✉ & Mohini M. Sain[1,4]

In this work, we set out to elucidate the light-harvesting properties of various random and ordered photocatalyst supports (PSs) with different macropore sizes. To accomplish this, we propose two studies of increasing relevance, enabled by computed tomography (CT) reconstructions and ray-tracing COMSOL Multiphysics simulations: (a) a 360-degree light release study approximating a PS situated within a compound parabolic concentrator (CPC) or cylindrical LED reactor with open ends; and (b) the same system as before but with closed ends. The ordered geometry is of interest, as it can be 3D printed at scale with a tailored morphology and porosity, and it can potentially be refined using machine learning models to optimize its light-harvesting properties. As will be shown, the local volumetric light absorption (LVLA) data suggests that an ordered PS with a more open pore interior and a smaller pore exterior would begin to approach the more isophotonic light-harvesting properties of random PSs.

Global markets will increasingly rely on energy vectors such as hydrogen for de-fossilizing our products and services. Heterogeneous photocatalysis provides one avenue for producing sustainable hydrogen from hydrogen carriers such as methanol, dimethyl ether, ethane, and ammonia. However, despite decades of research, the promise of de-fossilizing the chemicals and energy industries using solar-powered processes has suffered from low efficiency and thus has not been realized at any meaningful technological scale. Herein, we endeavor to address one aspect of the overall photocatalytic efficiency (defined as products formed over the incident photons), namely the local volumetric light absorption (LVLA), that needs to be characterized better. The International Union of Pure and Applied Chemistry's (IUPAC) definition for this quantity is the absorbed local spectral photon flux density or local volumetric rate of photon absorption, $L^a_{p,\lambda}(x,t)$ with units of mol_{photon} s^{-1} m^{-4}. An isophotonic photoreactor is one with zero or small gradient in the LVLA[1]. Please refer to Braslavsky et al. for more details of recommended terms for photocatalysis and radiation catalysis[2]. Optimization of the absorption of every photon collected by these processes is essential.

Photocatalysis, requires a thoughtful design of photoreactor and PS systems that allow for high photonic and, more broadly, high photocatalytic efficiency and allow appreciable light penetration throughout a photoactive surface area or volume. The radiation transport efficiency is defined as the ratio between the number of photons absorbed in the reactor volume at the specific wavelength and the number of photons sent into the reactor aperture by the employed light source[1]. While photoreactors should achieve a high radiation transport and subsequent photocatalytic efficiencies, low gradients in LVLA are desirable, i.e. striving for more isophotonic conditions in the reactor volume. This is in addition to thermochemical considerations such as limiting heat and mass transfer gradients and approaching ideal reactor flow fields for accurate and reproducible reactor/catalyst performance. Assuming the conventional considerations are met, we can begin to optimize photocatalysts by loading them onto reticulated porous PS structures, but this in turn requires quantification of their LVLA.

We use the term PSs to describe the macroporous foams herein. IUPAC classifies pores into three categories: micropores (below 2 nm in diameter), mesopore (between 2 and 50 nm) and macropores (greater than 50 nm) or in our case on the ~mm scale[3]. The problem with scaling photocatalytic systems is the various inefficient light-harvesting properties that we will define next. The term 'photonic' means the amount of incident photons arriving at the PSs' surface at the internal surface of the irradiation window

prior to absorption[2]. The ratio between the rate of reaction of the photocatalyst (loaded or intrinsic to the PS) and the incident photon flux inside the window of the reactor prior to absorption is called the photonic yield when the absorption is monochromic, and photonic efficiency when the absorption is within a defined wavelength interval[2]. Photocatalytic efficiency is broader, considering the energy out (product formed or reactant disappearing) over the energy in, the latter from *outside* the irradiation window and prior to absorption[2]. When considering a PS, Van Gerven et al.[4] defined illumination efficiency (η_{ill}) as:

$$\eta_{ill}(\%) = \kappa \cdot \left(\frac{P_{cat}}{P_{lamp}} \right) \cdot \left(\frac{A_{min\,E}}{A_{cat}} \right) \qquad (1)$$

where the unit of η_{ill} is m^{-1}, κ is the illuminated surface per unit of internal gas or liquid volume inside the reactor (m$_{ill}^2 \cdot$ m$_{reactor}^{-3}$ or m^{-1}), P_{cat} is the radiant power incident on the PS surface (W), P_{lamp} is the radiant power emitted from the lamp or light source (W), $A_{min\,E}$ is the PS surface area that receives at least the band-gap energy (m^2), and A_{cat} is the total PS surface area (m^2). In this work, LVLA represents the $A_{min\,E}$ term and is later quantified by the intensity of light absorbed on the volume sections of the PS. The PS's approximate photocatalyst supports with loaded photocatalyst by modifying its surface reflectivity between 30 and 90%.

Ineffectiveness in these properties translates into low photon-to-product efficiencies (<10%) that result in technologies that are too costly for commercialization[5]. The unofficial 'first law of photochemistry' says that a photon must be absorbed first to be effective[2]. An absorbed photon's properties are often referred to as its 'quantum' properties. There is thus a two-fold challenge: (a) optimizing the photonic properties of the PS; such as a low gradient in LVLA and a high radiation transport efficiency and (b) optimizing the photocatalyst material's quantum properties such as quantum yield or efficiency, depending on the monochromic or defined wavelength interval distinction mentioned earlier.

Herein, we focus on the PS architecture for photoactive materials with the goal of optimizing their light-harvesting properties, the results of which should be relevant to any PS system. The motivation for this study stems from our past experiences in the field of photocatalysts, where the catalysts we tested were in the form of particulates or loaded on PS materials, and the reaction rate was typically normalized with respect to surface area. Building on these experiences and our desire to characterize photocatalysts more rigorously, has led us to endeavor to quantify light absorption quantitatively throughout photoactive materials.

Light from light-emitting diodes (LEDs) is also expected to play a larger role in the future by allowing photo-assisted processes to run continuously. To be competitive with thermal or other electromagnetic-assisted processes (microwave assisted etc.), metrics such as wall-plug efficiencies need to be maximized. For instance, blue and near-ultraviolet (UV) (300–400 nm or ~UV-A) LEDs already exhibit the highest wall-plug efficiencies of over 90%, while the deep-UV LED regions are expected to improve from 5% (~ UV-B) and 15% (200–280 nm or UV-C) today to 76–90%, comparable to those of visible LED photons, by years 2030–2035[6]. As discussed in[6], the absorption of photons needs to be optimized for each application through photocatalyst design, their PS, and reactor design, and instead of providing only electrical heating (via photovoltaics), the photons can simultaneously drive excited-state photochemical processes and indirect photothermal heating. Ultimately, the cost of a mole of photons compared to a mole of product is a key economic performance metric of photocatalytic processes.

The approach adopted in this work is to characterize the light-harvesting properties of reticulated ceramic PSs with porosities that permit incident light access to the internal volume and active surface area. The PS struts can act either as a support for the photocatalyst or function as the photocatalyst itself (intrinsic).

Recent studies by Díez et al.[7] and Schreck et al.[8] summarized the many different types of PSs that have been tried: thin films[8], foams[8] (including ceramics[7]), sponges[8], silica[7] (including mesoporous[8]), quartz[7], cellulose[7],

electro-spun nanofibers[8], hydroxyapatite[8], macroscopic 3D structures made in part or entirely of photocatalytic materials[8] such as lignin or functional lignin as an ink binder[9], monolithic aerogels[8], inert 3D polymeric structures as scaffolds for nanoparticle-based aerogels[8] etc., photocatalyst shapes[7] (plates, spheres, rods, foams etc.), and photoreactors[7] (rotating discs, microreactors, monoliths etc.). They conclude that mass and photon transport remain the main challenges. Diez et al. employed a UV-TiO$_2$-coated and visible-Fe$_2$O$_3$-coated static mixer for aqueous photo-antibiotic degradation to attempt to address these concerns. Immobilizing the photocatalyst in this way eliminated the need for costly separation, and Diez and coworkers were able to operate in a laminar flow regime, saving pumping costs. They tried spray and dip coating techniques and found that the former led to a better TiO$_2$ film morphology that enhanced activity, while increasing the number of static mixers in series had no effect, suggesting the mass transfer was not limiting. In a comprehensive review, Danfá et al.[10] discussed TiO$_2$ supports and immobilization techniques and stated that ceramic PS materials stand out, because they are inexpensive and earth-abundant, and they have porosity that can be controlled and have good thermal, chemical, and mechanical stability. The authors outlined further criteria for optimum photocatalyst-support interaction, including (a) the preference of strong adhesion, (b) no degradation of activity or detrimental support effects, (c) high specific surface area, and (d) strong adsorption properties for reactants. Matter et al.[11] highlighted and Schreck et al.[8] demonstrated the multifaceted interplay between the photocatalyst geometry, PS, reactor design, and the light source when optimizing 3D photocatalysis. Ceramics materials, for example, can be printed via viscosity-controlled extrusion methods such as fused deposition modeling (FDM) or sintering methods such as selective laser melting or sintering (SLS). The former method uses a specialized ceramic-infused filament consisting of ceramic powder and thermoplastic binder and is the more common technique[12]. Formulating the right mixture ratio for FDM that preserves the ceramic's properties post-printing and meeting the specific printing process requirements while allowing for design flexibility are challenges for this method[12]. Alternatively, SLS's high sintering temperatures may limit direct incorporation of photocatalysts into the printed support structure, however, the print resolution is superior[12]. Both methods have trade-offs in affordability (FDM > SLS), build space (SLS > FDM), and resolution (SLS > FDM) as comprehensively reviewed here[12,13].

A 2009 study[14], assessed the unidirectional UV-assisted light source for degradation of aqueous organics using a P25 TiO$_2$ nano-powder coated on 15-, 20-, and 25-pore-per-inch (ppi) random alumina PSs. They found, upon illumination from a single incident angle, a 75% enhancement in catalyst-mass-normalized-phenol-mineralization activity for a 67% overall increase in pore size (25–15 ppi) or a slight super-linear (1.1-fold) activity change with pore size. A more recent 2019 study[15] quantified the unidirectional PS light-harvesting properties of a 3D TiO$_2$@Si monolith with an average mesopore size of ~2 μm (or 12,700 ppi), and porosity of 75%. In that study, the authors used a simultaneous spatial and time-resolved setup to measure light decay profiles after rapid pulses (300 fs) of laser light at 515 nm. They compared mesoporous supported and unsupported TiO$_2$ catalyst particles. They found that the supported photocatalyst allowed ~10-fold the light penetration and concluded that the reduction in bouncing frequency favored enhanced photon transport.

Methods

Simulation objectives and methods

Herein, we perform a 3D light simulation where we impinge the PSs with a light source approximating a CPC or cylindrical LED source.

Previous experimental studies

We can compare these results to our 2022 work[16] on solar-assisted CO$_2$ utilization via the RWGS reaction using indium-oxide hydroxide nanorods loaded on porous Ni-PSs illuminated by a low-concentrating CPC. In that study, we found that the catalyst's mass-normalized activity increased 1.94-fold for a 2.4-fold increase in pore size (0.23 to 0.56 mm or 110 to 45 ppi)

using a CPC reflector. We credited the better PS light-harvesting properties to a qualitative understanding that larger pores should allow more extensive 'light scattering-reflection events'[16].

PS evaluation and objectives

The properties of light in the PSs are evaluated using optical physics ray-tracing modeling for different pore sizes in COMSOL Multiphysics software, specifically the ray-optics module. There are few studies that predate this report based on cuboid PSs that used Monte Carlo ray-tracing techniques and sought to understand PSs radiative properties above 1000 K[17]. In the work described herein, we use the ray-tracing module of the COMSOL Multiphysics software to quantify the light-harvesting properties of cylindrical PSs. In both studies, the light is released from a three-dimensional (3D) light release feature that approximates a CPC. A detailed description of the ray-tracing theory can be found in the module's user guide. In this work a simple approach can be used to describe the propagation of light inside the simulation domain, since all surfaces are fully opaque, and no phase change occurs in between. For this reason, no refraction or volumetric scattering and absorption need to be modeled. Upon interacting with a surface, i.e. being reflected, a ray's path subsequent direction is defined only by its incident angle and the diffusive or specular nature of the surface's reflectivity. In this way the simulation can model the propagation of a light ray for an arbitrary number of interactions. To answer the question of where the light is absorbed inside the reaction volume, any value for the surface's total reflectivity can be mapped onto the ray path in post processing. For this a reflection law is used, Eq. (2), by which a reflected ray's intensity I is the result of the incident intensity I_0 multiplied by the total reflectivity R, with the latter being made up by a combination of a specular and diffusive share.

$$I = I_0 R \qquad (2)$$

Later we describe in detail the measurements of the PS' surface's optical properties, that show the specular share is very low, which is why it was neglected for a first approach. Accordingly, in COMSOL for all surfaces the "Wall" feature is chosen and the surface boundary condition is set to "diffuse scattering".

Study methods and procedures

The PS dimensions investigated in this study are ~10 mm diameter by ~15 mm length. Two random porosity PSs were analyzed, namely 10 and 15 ppi, along with an ordered PS of ~15.9 ppi. The analysis was conducted on bare uncoated PSs; however, we can approximate the influence of the optical properties of a photocatalyst surface layer on the light transport in the PS by changing the reflectivity of the PS surface.

The steps used for this analysis were:
a. Collect high-resolution 3D CT scans of the PSs using a Bruker SkyScan 1172 / Micro-CT system.

b. Reconstruct the 2D slices into a 3D Standard Tessellation Language (STL) CAD format using Fiji ImageJ2 v2.3.0/1.54 f.
c. Import the STL model into COMSOL Multiphysics v6.1 and mesh it.
d. Conduct ray-tracing simulations using the Ray Tracing module in the Geometrical Optics package of COMSOL Multiphysics.

The ceramic PS material used in this study was a reticulated (inter-connected) porous aluminum oxide (or alumina α-Al_2O_3 from ASK Chemicals LLC, Alfred, N.Y., U.S.A.) with a bulk density of 15–20% ceramic and 80–85% pore volume (air), with no more than 10% blocked pores (ASK Chemicals correspondence).

For an example of the procedure to convert CT images into a mesh in COMSOL, please refer to the Supplementary Methods section. As mentioned, three PSs were investigated, as shown in Table 1. Please see Supplementary Table S1 for mesh statistics.

PS properties

The scanning electron microscopy (SEM) images of the 10-ppi PS at two resolutions are shown in Fig. 1a, b. The reflectivity properties of the alumina ceramic PS were determined using a Lambda 1050 Integrating Sphere UV-Vis Spectrophotometer. The first sample measured was a flat slab sample of alumina from the original manufacturer (OM) of the porous PSs (ASK Chemicals). A second alumina sample was procured from another supplier, AdValue, and was measured as well. For the OM sample, triplicate measurements were taken of three relatively flat points on the surface and averaged, while for the AdValue sample; one measurement was taken at three different locations due to the low noise of the measurement. The PS materials were found to have reflectivities as shown in Fig. 1c, d.

Due to the large differences seen between the two manufacturers (Fig. 1c, d), it seemed prudent to make use of the OM material properties as much as possible. The diffuse component of the alumina scattering was also measured at near 100%. As can be seen in the above Fig. 1c, below about 400 nm, the OM alumina PS material begins to fluoresce, causing the reflectivity to register above 100% in the near-UV. Thus, to avoid this added complexity, all ray-tracing simulations were conducted at monochromatic 400 nm wavelength, where the reflectivity value was well defined near ~95% for the bare PS.

To validate that the simulated PSs were a suitable representation of the physical PSs, the reconstructed surface STL models were shrunk using SolidWorks to the dimensions of the physical PSs (~10 mm diameter). The original CT scans had a resolution of 11.56 μm per pixel; thus, any features less than this were not resolvable. Upon reconstructing the PSs, slightly reduced resolutions (45 and 55% of the original tomography scans for the 15 and 10 ppi, respectively) had to be used, as the reconstructed STL files would be too large for import into COMSOL otherwise. These resolutions result in feature sizes of 25.5 and 20.9 μm, respectively. Although the SEM images of the PSs show sub-20 μm features, the ceramic 3D-printing technique SLS can achieve resolutions down to 20–100 μm, thus any mass production process would achieve similar reconstructed PS resolutions investigated

Table 1 | Relevant PS dimensions

| Parameter	Identifier (ppi)	10 ppi (10)	15 ppi (15)	8 mm (15.9)
PS type	Random or ordered	Random	Random	Ordered
Macro-pore size	mm pore^{-1}	2.54	1.69	1.60
Resolution compared to original CT scan	%	55.0	45.0	Na
PS resolution	μm pixel^{-1}	20.9	25.5	Na
PS diameter in COMSOL (Average of x and y extents)	mm	10.0	10.0	10.0
PS height in COMSOL (z-axis extent)	mm	14.9	16.5	10.0
Light distance as a percent of PS dia.	%	30.0	30.0	30.0
Surface area	mm^2	1111	1668	978
Surface-area-to-volume ratio (apparent)	m^2 m^{-3}	949.4	1287.1	1244.7

Na not applicable.
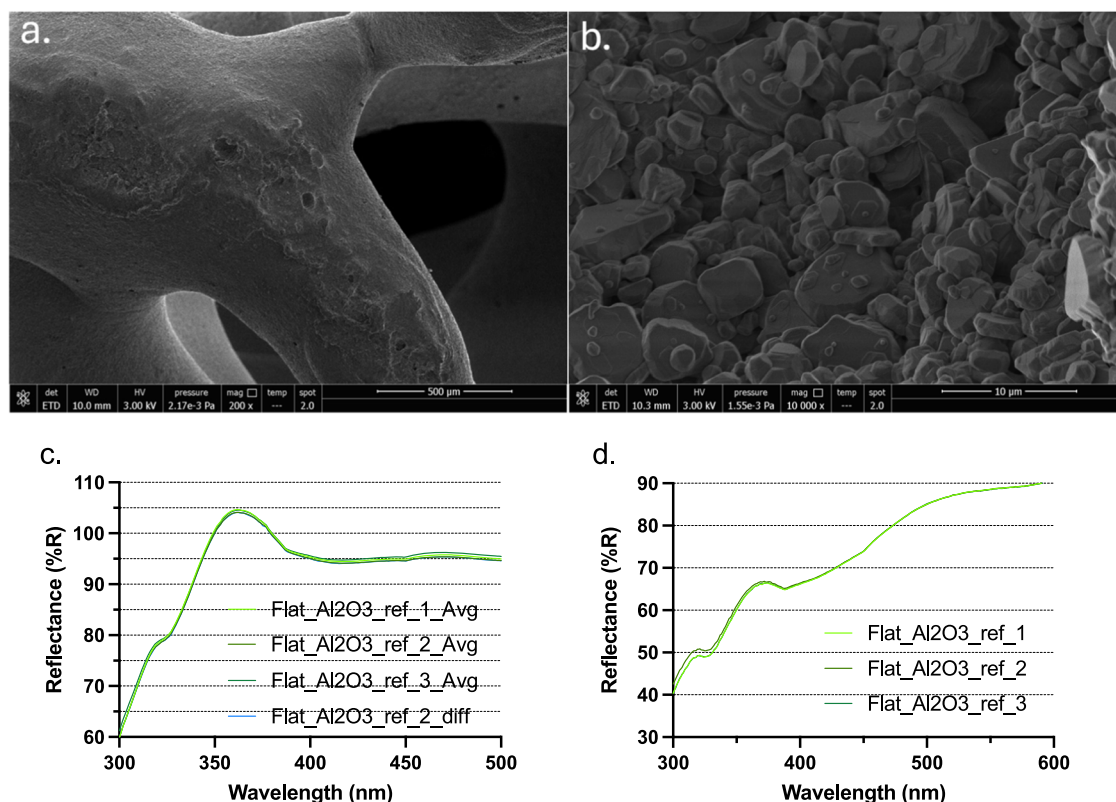
Fig. 1 | Bare alumina ceramic 10-ppi PS SEM images and two alumina manufacturers' reflectivity profiles. a macro pores (**b**) surface resolved. Reflectivity of alumina material from two suppliers, (**c**) ASK Chemicals (OM of alumina PSs), (**d**) AdValue (an alternative alumina supplier).

Table 2 | Assumptions of the two studies

Study	Study details
(1) 3D ray study (open cylinder)	a) 360° cylindrical ray release feature with open ends b) The ray-release feature located 30% of the PS's diameter away from the outer surface c) Released 2000 total rays in 4 quadrants around the PSs or 500 rays per quadrant d) Random 10/15 ppi and ordered (8 mm or 15.9 ppi) pore sizes e) Shrunk to physical PS size (~ 10 mm dia.) f) Fixed ray propagation length (0.1 mm step size and 400 mm max. propagation length) g) Single wavelength (400 nm) monochromatic h) Cylinder wall with reflectivity of 100% i) Rays reflected diffusely from both PS and cylinder walls j) Ray trajectories exported and end points inside the PS geometry and binned as a function of interactions k) Interaction points plotted as a function of equal volume cylindrical PS segments or radii l) Rays allowed to interact a minimum of 5 or 8 times m) When all rays in the simulation achieve a minimum 5 or 8 interactions the simulation stops. This can allow more but not less total interactions per ray n) Photocatalyst reflectivity cases of 30, 50, and 90% plotted approximating a PS with different photocatalyst layer properties o) Bounding box surrounding system to limit ray propagation outside bounds p) Please see Supplementary Discussion for details about the start/stop conditions
(2) 3D ray study (closed cylinder)	a) 3D cylindrical ray release feature with closed ends b) End caps located adjacent to PS ends (no gap) c) End caps have reflectivity of 100% and do not emit light d) Two additional ordered (Hyb1 & Hyb2) PSs analyzed e) Same b) to p) as previous study

herein[13]. To confirm that we were not adding extraneous error to the surface area at the reduced resolutions, two resolutions (45 and 55%) of the 10 ppi were examined and were found to deviate <3%. An ordered PS called '8 mm' was also examined for its light-harvesting properties, as this type of PS may be amenable to rapid scaling by 3D printing. The '8 mm' description is due to making 5 × 8 mm through-holes of a 50-mm diameter PS in TinkerCAD. This was also shrunk to the random PS dimensions.

The threshold of the reconstructed PS was also a parameter in Fiji (ImageJ) when reconstructing the STL files from CT data. The optimum threshold value used was 20%, which resulted in the least number of free particles (requiring the least deletions in COMSOL) and the best meshing likelihood for both random PSs. The threshold value affected the geometry surface area only marginally (< few %) at the resolutions used.

The relevant PS resolutions used in the simulations are shown in Table 1 and were slightly different based on COMSOL's ability to successfully import a given resolution. Two studies were conducted, as shown in Table 2. The objective was to provide some quantitative understanding of the PS light-harvesting properties. Each study will be discussed in subsequent sections.
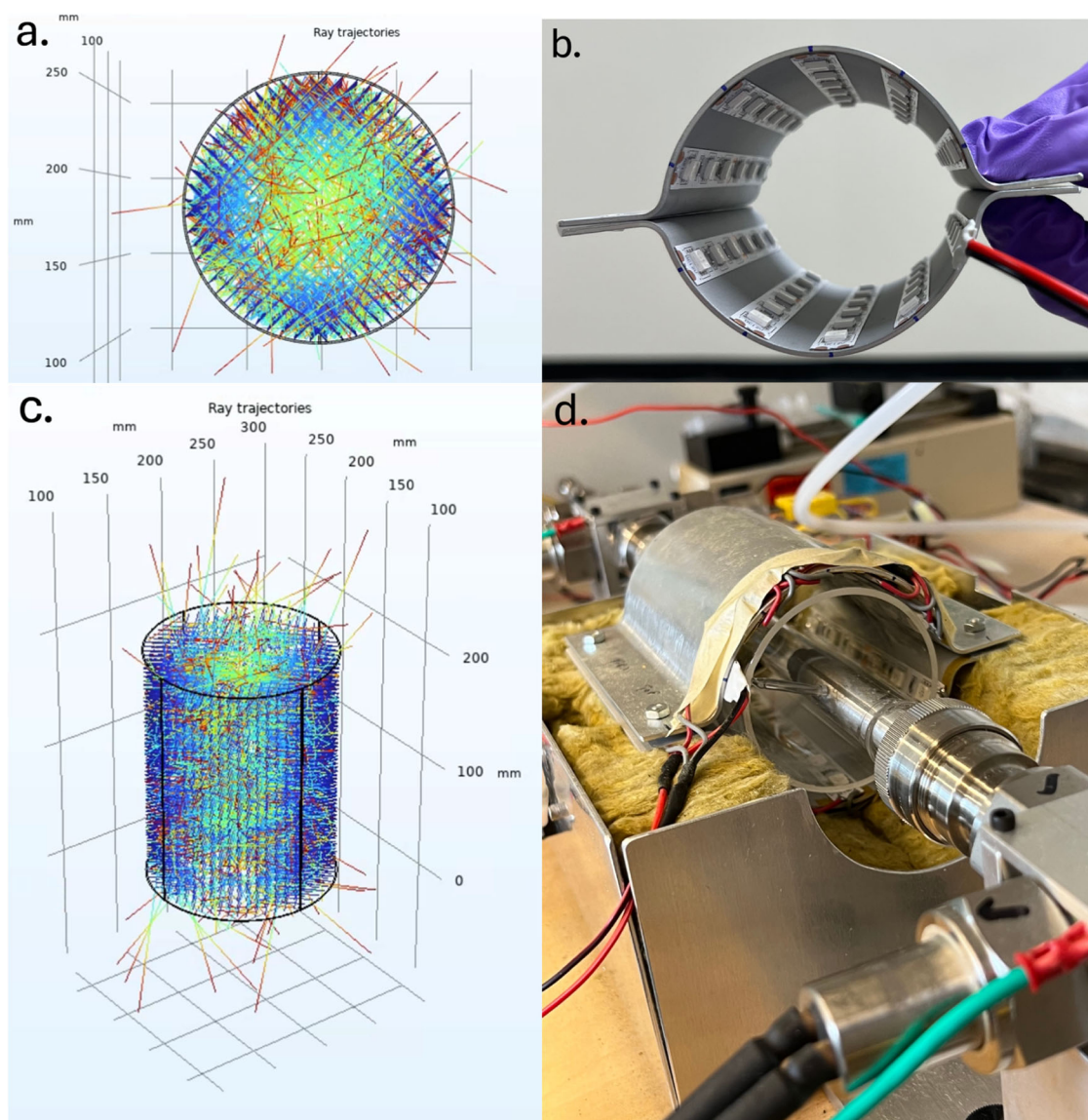
Fig. 2 | Experimental photoreformer reactor as an example of an analogue for the light-release feature and configuration. a Birds-eye view of simulated PS visualized in COMSOL, (**b**) approximately matching an experimental system's light-release feature being built in parallel for photo-reforming reactions in our laboratory (Ozin and Sain groups), (**c**) perspective view of light-release feature with PS inside cylinder visualized in COMSOL, (**d**) experimental integration of cylindrical light source and PS in a prototype photo-reforming reactor system being built in our laboratory.

In the simulations, the light scattering was assumed to be diffuse, and only one ray is reflected for each ray. The simulations results were based on an incident light wavelength of 400 nm and a total light path length of 400 mm with a specified 0.1 mm step size (discretization step size), which were used for all simulations. Once the interactions were binned, the PSs were modeled using reflectivities of 30, 50, and 90% which meant that multiple scatters would diminish the ray intensity differently for a given reflectivity, causing its intensity to diminish slower (90%) or faster (30%) for a certain number of interactions. Please see Supplementary Information for more details.

It is expected that the incident light will scatter more in the smaller pores with closer proximity struts of the PS, thereby diminishing faster. The likelihood of enhanced light-harvesting properties in the smaller pores requires further investigation. The opposite is expected of the larger pore sizes, i.e. the number of rays remaining would be expected to have statistically scattered less and have higher final intensity by the same path length or lifetime. Each location of rays' reflection on a surface indicates that energy could be harvested in the form of photochemical or non-radiative relaxation (otherwise known as photothermal heating) in these regions.

Results

Study 1: 3D ray study with cylindrical ray release feature and open cylinder

Due to the practical interest surrounding intensification for photo-assisted processes, approaches that maximize light harvesting were investigated. The PSs were devised to be surrounded by a slightly larger concentric cylinder, which simulated where 3D light rays propagated from (Fig. 2a, c), an analog for a CPC or LED reactor device (Fig. 2b, d). Work on experimental photoreactor analogs such as the photo-reformer system in Fig. 2 that combine all aspects of this study with LED and photocatalyst optical properties and activity is ongoing and will be used to verify and further confirm the simulation results in future reports. The LVLA characteristics of the PSs discussed herein (corroborated by actinometry data) feed into the external quantum efficiency calculation (using LED properties, reactor geometry, and reactor losses to determine incident photons to absorbed photons) for ultimately maximizing the photon-to-product efficiency which needs to exceed ~10% for a photochemical system to be commercially viable[5]. This efficiency has been estimated based on capital and operating equipment costs to product proceeds[5] and the methodology is applicable to any new
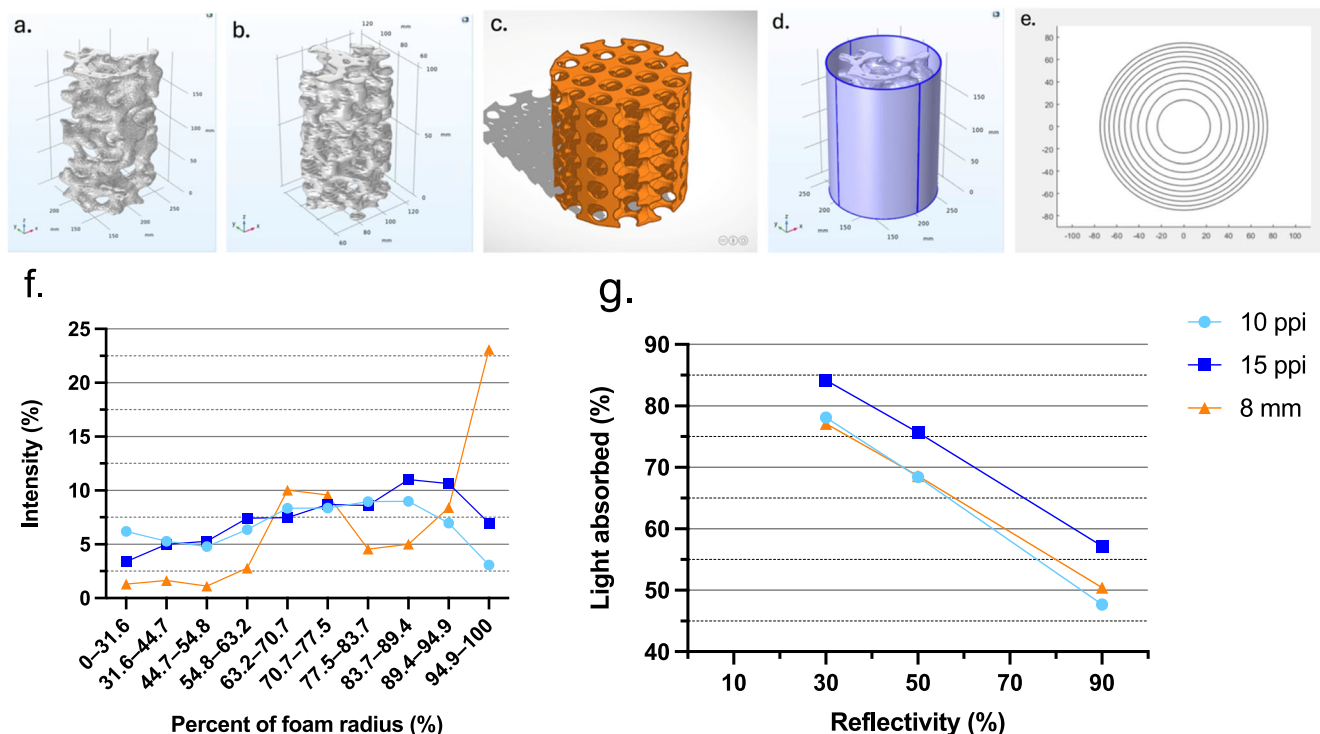
Fig. 3 | Random and ordered PSs with modelled light release feature and volume segments for open cylinder ray-tracing study. a Random 10-ppi PS, (**b**) random 15-ppi PS, (**c**) 8 mm ordered through-hole geometry (made with TinkerCAD), (**d**) random 10-ppi PS shown with open light release cylinder, (**e**) PS equal volume segments or volume sections, (**f**) study 1 average ray intensities (or light absorption) of incident radiation as a function of PS volume sections for 50% reflectivity, (**g**) study 1 plot of incident light captured as a function of reflectivity on x-axis.

photoreactor and PS system. To allow direct comparison between different PS resolutions, the ray release cylinders were situated at 30% of the PS's average x and y diameters from the PS surface. The light release walls were set to a diffuse reflectivity of 100%. In practice, an anodization surface treatment of alumina can result in a maximum diffuse reflectivity of around 80% for white light. However, for comparison purposes, the reflectivity of the wall was assumed to be lossless (reflectivity of 100%). Thus, the simulation can complete once all the rays have achieved a minimum ray interaction count of 5 or 8 with the PS or cylinder walls, or both, whereby all rays kept propagating until they all achieved an interaction count above the certain specified threshold or when they escaped at the open ends and terminated at the bounding box. The total rays' intensities were not specified or computed by COMSOL whereby the simulation stop condition was as described above. After completion of the simulation the ray trajectories were exported and the interactions with the PSs were binned and thus the intensities were determined as a function of PS radius. Please refer the Supplementary sections 'Assumptions for simulation stop conditions' including Figs. S1–S7 and Tables S2–S8.

To estimate where inside the PSs the rays are absorbed, the ray interactions (counted in bins) were plotted against constant volume segments. The ray count was 500 rays per quadrant (RPQ) for a total of 2000 rays. The three simulated PSs (10, 15 ppi random and 8 mm ordered geometry) are shown in Fig. 3a–c. RPQ is a designation used in this analysis as the light source is split up into four quadrants as shown in Fig. 3d, whereby each quadrant was initialized with an equal number of rays which propagate from them in a randomized way. A visual representation of the constant volume segments of the PS is depicted in Fig. 3e, which can be plotted on the x-axis as volume sections. The average intensities determined from the interaction counts are shown in Fig. 3f, and the average incident light captured is shown in Fig. 3g.

The three PSs compared in study 1 were surrounded in COMSOL by a cylindrical light release feature with four quadrants and with open ends as shown in Fig. 3d. Average incident intensities as a function of the PS radius were assumed to have been absorbed on the surface, and those outside the z-axis extent (top and bottom) of the PS were assumed lost out the open ends. The cases shown in Fig. 3f are the 50% reflectivity scenario, whereby an absorbing photocatalyst layer is assumed to be present. The analysis shows that the smaller-pore PS (15 ppi or more pores per inch) traps light slightly better in the exterior volume sections (>83.7–100%) than the larger-pore PS (10 ppi or less pores per inch), and both showed similar LVLA profiles from volume sections 31.6–83.7% while the 10-ppi absorbed slightly better in the interior (<31.6%). The two PSs behave in such a way that past a certain inner volume section/radius (~ 83.7%), the light gets trapped well (which implies the PS is doing the light trapping), while above this threshold, the light can more easily escape, and the intensity diminishes toward the surface. The 10-ppi and 15-ppi PSs for study 1 absorbed 67.35 and 74.49% of the total incident intensity on their surfaces, respectively, while the ordered (8 mm) PS achieved 67.53% overall. Below the mid-volume point (≤70.7% radius), the 10- and 15-ppi PSs average light intensities (or light absorption) were 6.20 and 5.71% per volume section, respectively, and above that point to the surface, the average intensities were 7.27 and 9.18% per volume section, respectively. The corresponding average intensities less than and above the mid-volume point for the ordered PS are 3.37 and 10.13%, respectively. To verify these values, if the average is taken of the two volume sections above and below 70.7% radius the total absorbed of incident light is calculated by multiplying by 10 total volume sections. The ordered (8 mm) PS, in general, fared poorly compared to the random PSs, showing uneven light distribution for the LVLA. For the random PSs, the LVLA profiles have implications for the photocatalyst architecture and loading approaches to maximize catalyst absorption, due to light absorption differences in outer volume vs. inner volume sections with different pore size. Figure 3g shows the light capture as a function of reflectivity, and as can be seen lower reflectivity allows more light capture for study 1. Because of the open-ended cylinder for this study, for the 30, 50, and 90% reflectivity cases, 16–23, 24–31, and 42–51% of the incident rays were lost out of the ends. In
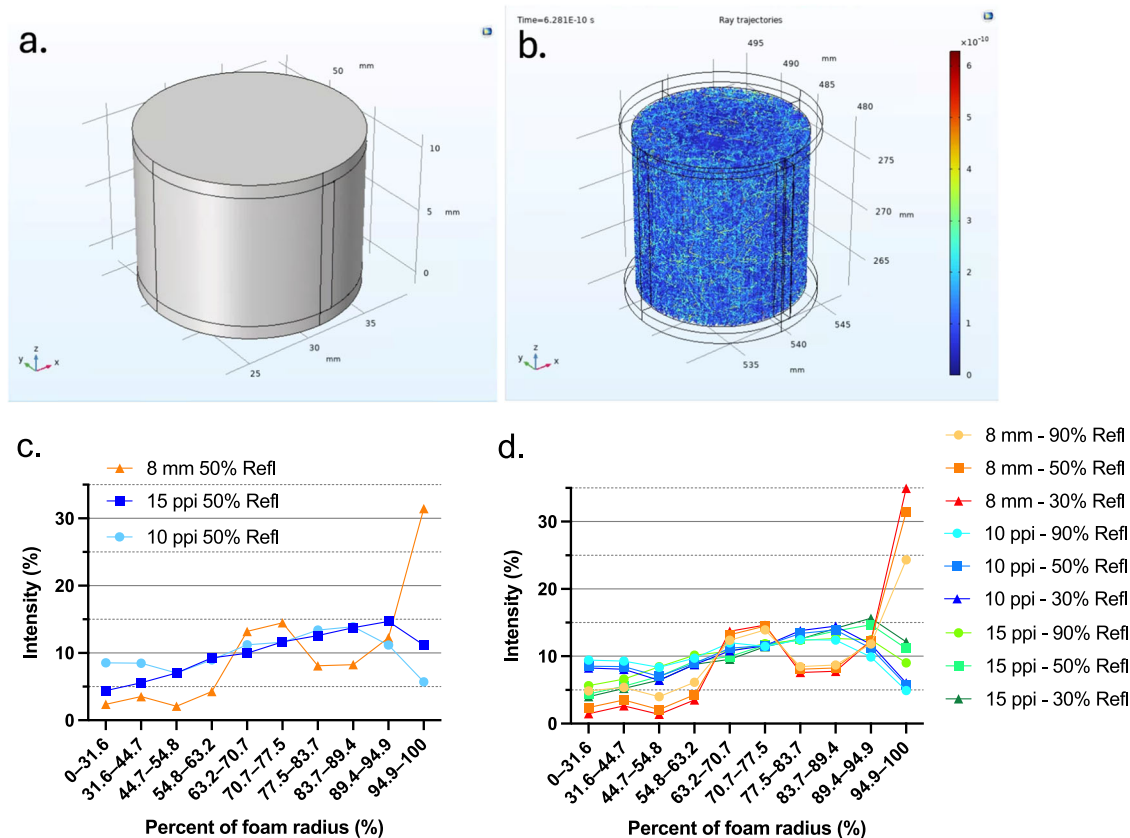
Fig. 4 | Random and ordered PSs used in closed cylinder ray-tracing study. a PS containment geometry, (**b**) Light propagation up to minimum 5 or 8 interactions within the reactor volume with closed ends, normalized to 100% as all light is assumed captured, (**c**) PS average intensity (or light absorption) as a function of PS equal-volume sections (**d**) PS average intensity as a function of photocatalyst layer reflectivity and equal volume sections.

the next study, we will attempt to quantify the isophotonic characteristics of these PSs without light losses, whereby they can be more accurately compared.

Study 2: 3D ray study with cylindrical ray release feature and closed cylinder

A light 'fingerprint' of the various PSs was produced by confining the propagating rays to the photoreactor and PS surface by sealing the end caps (Fig. 4a). This approximates what a perfect photoreactor would attempt to achieve such that no photons are left behind. (Fig. 4b). The wall was again assumed to be lossless in its reflectivity (100%) and to reflect light diffusely, and the PS was assumed to have a reflectivity of 30–90%. The light release was again on the inner cylindrical surface in four quadrants, while the top and bottom lids were 100% reflectors and not light emitters. This approximates an idealized photoreactor/PS/photocatalyst system with a photocatalyst layer of some reflectivity. As before, the number of rays for these simulations was 500 RPQ for a total of 2000 rays each.

What can be observed from this analysis (Fig. 4c) is that again the random PSs show the same monotonic decrease in absorption toward the outer volume sections, but interestingly, the 10-ppi PS absorbed light slightly better in the interior than the 15-ppi PS, while in the outer volume sections, there is a crossover whereby the 15-ppi PS had better light absorption. Again, the ordered PS showed the best absorption at 70.7–77.5% volume section of all PSs tested; however, the absorption diminished in both directions away from this peak and was the least isophotonic overall. An ideal isophotonic profile would be a flat line at all radii, and the unoptimized random PSs do a fairly good job in this respect. The average light intensity over all PSs radii was 10.0% due to all rays remaining present, and the total was normalized to 100%. Below the mid-volume point, the 10- and 15-ppi PSs had average light intensities (or light absorption) of 8.84 and 7.23%, and

above that point (but below the surface), had average light intensities of 11.16 and 12.77%, respectively. Below and above the mid-volume point of the ordered PS, the average light intensities were 5.09 and 14.91%, respectively, both below the surface. Figure 4d show the light capture as a function of reflectivity. This has implications for designing ordered PSs that can be 3D printed, whereby they could be structured such that the outer radius has smaller pores while the interior opens into larger pores.

PS considerations for single-incident-angle photocatalysis

In terms of the limiting sizes for large- and small-pore PSs, for the former, appropriate strut size, strut robustness, and compression resistance would limit the maximum pore sizes, whereas pressure drop would become limiting factors for the latter. For smaller pore PSs, as was found in[15], the attenuation coefficient increases with decreasing pore size and becomes limiting for more light-harvesting. Interestingly, the ordered PS offers about the same surface-area-to-volume ratio as the 15-ppi random PS showing that similar ratios are achievable in both. Other considerations are that the light needs to impinge on the ordered-geometry PS at a particular angle: at 45° to the through-holes for optimal harvesting, while the random pores allow for more continuous incident angles, which is advantageous for less accurate optical-tracking setups vs. more accurate and expensive active-tracking. For example, the more flexible collectors could be low-concentration CPCs. This flexibility would allow random pores to be more convenient for light harvesting from all angles.

We return to our previous study's result that was mentioned in the introduction, in which we found that the catalyst's mass-normalized activity increased 1.94-fold for a 2.4-fold increase in pore size using a CPC reflector. It remains a challenge to provide a direct comparison, as the PS from that study was a nickel mesh wrapped around an inner heating cylindrical rod which was not porous to its interior (like herein). Furthermore, the

porosities were 0.23–0.56 mm compared to 1.69–2.54 mm here, presenting different attenuation coefficients whereby the light-harvesting properties differ. Further, the reflectivity/absorption coefficient of the catalyst was not measured in that study and could vary considerably from the 30–90% used here. Finally, the more open-pore PS did not harvest light better in the exterior for both studies considered here. Therefore, the nearest comparison that can be made is from the 2nd study herein comparing the interior light harvesting where the 10-ppi PS harvested 1.22-fold (8.84 vs. 7.23% absorption) better for a 1.5-fold increase in pore size (Table 1). The activity:porosity ratio matches the 0.81 in the previous study (also 0.81 here), resulting in analogous conclusions.

Ordered hybrid structures with cylindrical ray release feature and closed cylinder

Building on the results thus far, we hypothesize that an ordered hybrid-type PS could be constructed to potentially take advantage of the benefits of both

random PSs investigated. To this end, we applied a volumetric construction method using a commercial graphical software, Cinema 4D, to generate an ordered PS with two outer layers of 15-ppi spherical pores for light trapping, and two inner layers of 10-ppi spherical pores for light propagation. Specifically, layers of spatially distributed, interconnected spherical volumes were removed from a cylindrical volume, where the diameters of spheres were designed to decrease radially. These ordered 'hybrid-1' and 'hybrid-2' PSs are shown in Table 3 and Fig. 5a–d, where the 'negative' spherical volumes were slightly different. The effective structural difference between the two is that the latter had an optimized inner-pore-entrance pore size while the former did not. Please see Supplementary Table S1 for mesh statistics.

The LVLA results are shown in Fig. 6a, b. The outer layers did harvest light comparable to the random 15-ppi PS, while at intermediate radii they showed similar or better light absorption than both random PSs, but inferior in the interior. At the innermost radii, the optimized hybrid-2 PS

Table 3 | Relevant hybrid-PS dimensions

Parameter	Identifier (ppi)	Hybrid-1 (10/15)	Hybrid-2 (10/15)
PS type	Random or ordered	Ordered	Ordered
Macro-pore size	mm pore^{-1}	~1.69/2.54	~1.69/2.54
Resolution compared to original CT scan	%	Na	Na
PS resolution	μm pixel^{-1}	Na	Na
PS diameter in COMSOL (Average of x and y extents)	mm	10.0	10.0
PS height in COMSOL (z-axis extent)	mm	15.0	15.0
Light distance as a percent of PS dia.	%	30.0	30.0
Surface area	mm^2	1999	1888
Surface-area-to-volume ratio (apparent)	m^2 m^{-3}	1696.7	1602.4

Na not applicable.

Fig. 5 | Hybird PSs used in closed cylinder ray-tracing study. a, b Ordered hybrid-1 PS, (**c**) ordered hybrid-1 PS inner pores, (**d**) ordered hybrid-2 PS inner-pore-size optimization.
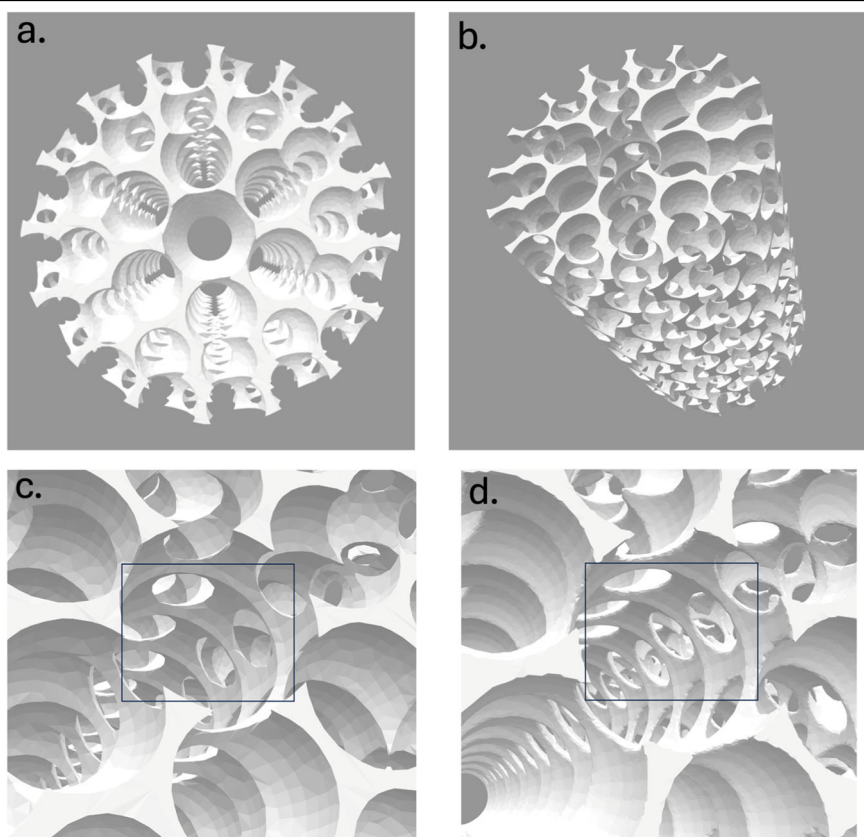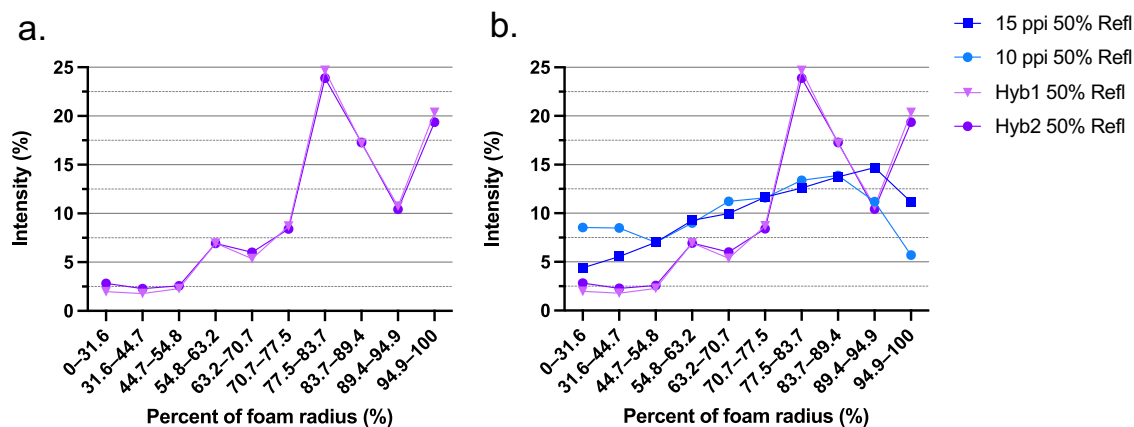
Fig. 6 | LVLA profiles for select PSs for closed cylinder ray-tracing study. a Ordered hybrid-1 and hybrid-2 LVLA, and b hybrid PSs compared to random PSs.

harvested light slightly better than the unoptimized hybrid-1 PS as expected, mirroring the inner-pore-light-harvesting effectiveness of the random 10-ppi PS. Overall, we have begun to show that by applying the lessons learned from the random-PS studies we can begin to construct ordered PSs that replicate the former's more isophotonic characteristics. More refined ordered geometries could be developed by applying ML to this optimization scheme, to achieve even more uniform LVLA, and can be tuned to photocatalyst-specific wavelengths and reflectivities (here 400 nm and 50% reflectivity).

Discussion

Here we first discuss the technical challenges of scaling ordered PSs. The adoption of 3D printing to produce ordered PSs introduces several technical challenges that must be addressed to ensure the viability and efficiency of these components in commercial settings. One significant concern is durability in real-world conditions, which involves the environmental stability and longevity of the PSs. These supports need to withstand extreme conditions such as fluctuating temperatures, continuous exposure to UV light, humidity, and potential chemical corrosives commonly found in industrial environments. The materials used must not only be resilient but also maintain their photocatalytic activity over extended periods to ensure long-term operational viability. Furthermore, integrating newly developed 3D printed PSs into existing photocatalytic systems poses its own set of challenges. Compatibility with current configurations is paramount; the PSs must fit seamlessly into established setups without necessitating significant modifications. This might involve customizing the design of the PSs to match specific reactor geometries or connection interfaces, which could add to the complexity and cost of production. Successfully overcoming these technical and integration challenges requires a multidisciplinary approach involving continuous innovation in 3D printing technology, rigorous testing and quality assurance, and thoughtful consideration of the regulatory landscape. Collaboration among researchers, industry experts, and regulatory bodies will be essential in advancing the commercial regulatory bodies will be essential in advancing the commercial application of 3D-printed PSs in photocatalysis.

To consolidate the analyses, we now present a visualization or a bigger picture of the overall properties and their effects on the goal of high photon-to-product efficiency (Fig. 7). The pertinent property groups include: the light, photoreactor, PS, photocatalyst, in no particular order. Study 1 considered a single wavelength, lossless photoreactor walls (100% reflectivity), and a homogeneous light source; however, due to the open containment of the photoreactor the resulting radiation transport efficiency was poor (<<100%). This study provided a baseline LVLA wherein the light and certain photoreactor properties were optimized, while the photoreactor containment was not. Study 2 again considered a single wavelength with

photoreactor walls and light properties optimized but differed in having a closed containment of the photoreactor. This study permitted the photons to absorb only on the PS surface and accordingly approached an ideal radiation transport efficiency of ~100%. Thus, this study provided a ceiling on the LVLA wherein the reactor and light properties were optimized, while the PS properties could be tuned. By systematically optimizing these four property groups, we can make further progress in designing and optimizing high-efficiency light-driven processes.

Using PSs requires that we characterize the theoretical and practical limits of their light-harvesting properties. Qualitatively and from experimental results, we expect larger porosity structures to allow more direct light penetration. It soon became apparent that calculating the PS's LVLA, obtained by counting ray absorption as a function of PS constant volume section or radius, was of utmost importance to quantify its isophotonic properties. In the open cylinder study 1, the smaller pore random PS (15 ppi) was found to harvest 74.49% of the incident light on all surfaces (vs. 67.35 (10 ppi) and 67.53% (8 mm ordered)) for a 50%-reflectivity photocatalyst layer, diminishing towards the surface for the random PSs. Notably, the 15-ppi PS had better light absorption at almost all radii compared to the 10-ppi and ordered PSs. In the closed cylinder study 2, where the light reflected continuously until it was absorbed on some surface of the PSs, on average the light absorption in the interior ($\leq$70.7%) for the 10-ppi PS exceeded the others at 8.84% (vs. 7.23 (15 ppi) and 5.09% (8 mm ordered)). The hybrid 1 and 2 PSs had the least average light intensities (or light absorption) in the interior ($\leq$70.7% at 3.67 and 4.13%, respectively) which means most absorption was in the exterior at 16.33 and 15.87%. In this second study, overall, the degree of isophotonic light harvesting of the PSs was quantified using the standard deviation (lower value is better) of the intensities at all radii and the 10-ppi PS was found to be slightly better than the 15-ppi PS (2.69 vs. 3.46% SD); however, the ordered foams have some way to go (8.81, 8.16, and 7.66% SD for the 8 mm, Hyb-1, and Hyb-2, respectively). The hybrid closed-cylinder study demonstrated that indeed ordered PSs can take advantage of random PS characteristics. With further optimization, ordered PSs may exhibit more uniform isophotonic properties than random PSs at all radii. Mass production of efficient, ordered PSs via 3D printing then becomes possible.

Future research in photocatalysis should focus on exploring non-traditional PS geometries and integrating hybrid materials to enhance efficiency and adaptability. Innovations such as fractal or biomimetic structures could offer superior light harvesting due to their expansive surface areas, while dynamic PS designs that adjust properties in response to environmental stimuli could maximize operational efficiency. Additionally, the use of hybrid materials combining different photocatalytic properties could facilitate improved electron transfer and overall system performance. This approach requires advanced computational modeling
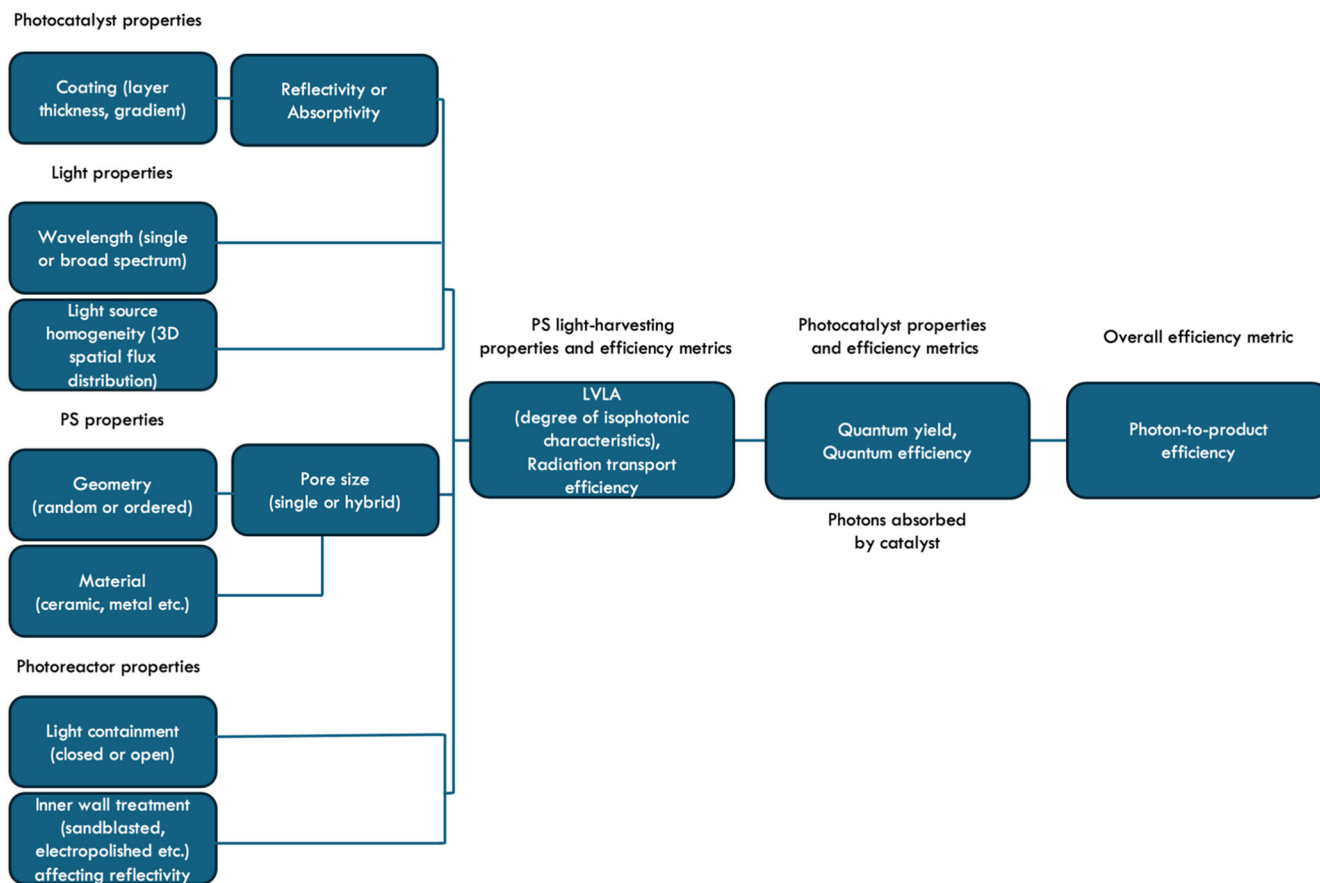
Fig. 7 | Optimizing photocatalytic processes.

and innovative manufacturing techniques, such as 3D printing capable of handling multiple materials, to ensure economic viability and environmental sustainability.

Data availability

The authors declare that the data supporting the findings of this study are available within the article and its supplementary information files or from the corresponding authors on reasonable request.

References

1. Kant, P. P. Optimizing photocatalysts and photoreactors for solar fuel synthesis. (Karlsruhe Institute of Technology, Karlsruhe, 2023).
2. Braslavsky, S. E. et al. Glossary of terms used in photocatalysis and radiation catalysis (IUPAC recommendations 2011). *Pure Appl. Chem.* **83**, 931–1014 (2011).
3. Li, X., Yu, J. & Jaroniec, M. Hierarchical photocatalysts. *Chem. Soc. Rev.* **45**, 2603–2636 (2016).
4. Van Gerven, T., Mul, G., Moulijn, J. & Stankiewicz, A. A review of intensification of photocatalytic processes. *Chem. Eng. Process. Process Intensif.* **46**, 781–789 (2007).
5. Stechel, E. B. & Miller, J. E. Re-energizing CO_2 to fuels with the sun: Issues of efficiency, scale, and economics. *J. CO2 Utilization* **1**, 28–36 (2013).
6. Schroeder, E. & Christopher, P. Chemical production using light: Are sustainable photons cheap enough? *ACS Energy Lett.* 880–884 https://doi.org/10.1021/acsenergylett.2c00142 (2022).
7. Díez, A. M. et al. A step forward in heterogeneous photocatalysis: Process intensification by using a static mixer as catalyst support. *Chem. Eng. J.* **343**, 597–606 (2018).
8. Schreck, M. et al. 3D printed scaffolds for monolithic aerogel photocatalysts with complex geometries. *Small* **17**, 1–12 (2021).
9. Jiang, B. et al. Wood-inspired binder enabled vertical 3D printing of g-C3N4/CNT arrays for highly efficient photoelectrochemical hydrogen evolution. *Adv. Funct. Mater.* **31**, 2105045 (2021).
10. Danfá, S., Martins, R. C., Quina, M. J. & Gomes, J. Supported TiO_2 in ceramic materials for the photocatalytic degradation of contaminants of emerging concern in liquid effluents: A review. *Molecules* **26**, (2021).
11. Matter, F. & Niederberger, M. The importance of the macroscopic geometry in gas-phase photocatalysis. *Adv. Sci.* **9**, 1–15 (2022).
12. Yusuf, A. O. et al. 3D Printing to enable photocatalytic process engineering: A critical assessment and perspective. *Appl. Mater. Today* **35**, 101940 (2023).
13. Friedmann, D., Lee, A. F., Wilson, K., Jalili, R. & Caruso, R. A. Printing approaches to inorganic semiconductor photocatalyst fabrication. *J. Mater. Chem. A* **7**, 10858–10878 (2019).
14. Plesch, G., Gorbár, M., Vogt, U. F., Jesenák, K. & Vargová, M. Reticulated macroporous ceramic foam supported TiO2 for photocatalytic applications. *Mater. Lett.* **63**, 461–463 (2009).
15. Bernadet, S. et al. Bulk photodriven CO_2 Conversion through TiO_2 @Si(HIPE) monolithic macrocellular foams. *Adv. Funct. Mater.* **29**, 1–8 (2019).
16. Hurtado, L. et al. Solar CO_2 hydrogenation by photocatalytic foams. *Chem. Eng. J.* 134864 https://doi.org/10.1016/j.cej.2022.134864 (2022).

17. Petrasch, J., Wyss, P. & Steinfeld, A. Tomography-based Monte Carlo determination of radiative properties of reticulate porous ceramics. *J. Quant. Spectrosc. Radiat. Transf.* **105**, 180–197 (2007).

Author contributions
A.A.T. conceived the analysis, carried out the simulations, wrote the paper and raised part of the funding. A.D. cowrote the paper, discussed the results, assisted with data analysis and verification with MATLAB, provided input for reviewer comments on ray-tracing theory, and provided critical feedback and simulation validation. W.Z. discussed the results, generated, and optimized the hybrid structures, edited the hybrid structure section, wrote the technical challenges section and part of the final discussion and provided critical feedback. A.M. discussed the results, provided input for reviewer comments, assisted with COMSOL simulation validation, and provided critical feedback. A.D. and A.M. performed the alumina reflectivity measurements. N.P.K. facilitated access to the COMSOL Multiphysics software. N.P.K., G.A.O. and M.M.S. provided funding sources, critical guidance, feedback, and advice.

Competing interests
The authors declare no competing interests.

Additional information
Supplementary information The online version contains supplementary material available at https://doi.org/10.1038/s41524-024-01409-0.

Correspondence and requests for materials should be addressed to Geoffrey A. Ozin.

Reprints and permissions information is available at http://www.nature.com/reprints

Publisher's note Springer Nature remains neutral with regard to jurisdictional claims in published maps and institutional affiliations.